Measurement of the Reactor Antineutrino Flux and Spectrum at Daya Bay

F. P. An,[1] A. B. Balantekin,[2] H. R. Band,[3] M. Bishai,[4] S. Blyth,[5,6] I. Butorov,[7] D. Cao,[8] G. F. Cao,[9] J. Cao,[9] W. R. Cen,[9] Y. L. Chan,[10] J. F. Chang,[9] L. C. Chang,[11] Y. Chang,[6] H. S. Chen,[9] Q. Y. Chen,[12] S. M. Chen,[13] Y. X. Chen,[14] Y. Chen,[15] J. H. Cheng,[11] J. Cheng,[12] Y. P. Cheng,[9] J. J. Cherwinka,[2] M. C. Chu,[10] J. P. Cummings,[16] J. de Arcos,[17] Z. Y. Deng,[9] X. F. Ding,[9] Y. Y. Ding,[9] M. V. Diwan,[4] J. Dove,[18] E. Draeger,[17] D. A. Dwyer,[19] W. R. Edwards,[19] S. R. Ely,[18] R. Gill,[4] M. Gonchar,[7] G. H. Gong,[13] H. Gong,[13] M. Grassi,[9] W. Q. Gu,[20] M. Y. Guan,[9] L. Guo,[13] X. H. Guo,[21] R. W. Hackenburg,[4] R. Han,[14] S. Hans,[4] M. He,[9] K. M. Heeger,[3] Y. K. Heng,[9] A. Higuera,[22] Y. K. Hor,[23] Y. B. Hsiung,[5] B. Z. Hu,[5] L. M. Hu,[4] L. J. Hu,[21] T. Hu,[9] W. Hu,[9] E. C. Huang,[18] H. X. Huang,[24] X. T. Huang,[12] P. Huber,[23] G. Hussain,[13] D. E. Jaffe,[4] P. Jaffke,[23] K. L. Jen,[11] S. Jetter,[9] X. P. Ji,[25,13] X. L. Ji,[9] J. B. Jiao,[12] R. A. Johnson,[26] L. Kang,[27] S. H. Kettell,[4] S. Kohn,[28] M. Kramer,[19,28] K. K. Kwan,[10] M. W. Kwok,[10] T. Kwok,[29] T. J. Langford,[3] K. Lau,[22] L. Lebanowski,[13] J. Lee,[19] R. T. Lei,[27] R. Leitner,[30] K. Y. Leung,[29] J. K. C. Leung,[29] C. A. Lewis,[2] D. J. Li,[31] F. Li,[9] G. S. Li,[20] Q. J. Li,[9] S. C. Li,[29] W. D. Li,[9] X. N. Li,[9] X. Q. Li,[25] Y. F. Li,[9] Z. B. Li,[32] H. Liang,[31] C. J. Lin,[19] G. L. Lin,[11] P. Y. Lin,[11] S. K. Lin,[22] J. J. Ling,[32,18,4] J. M. Link,[23] L. Littenberg,[4] B. R. Littlejohn,[26,17] D. W. Liu,[22] H. Liu,[22] J. L. Liu,[20] J. C. Liu,[9] S. S. Liu,[29] C. Lu,[33] H. Q. Lu,[9] J. S. Lu,[9] K. B. Luk,[28,19] Q. M. Ma,[9] X. Y. Ma,[9] X. B. Ma,[14] Y. Q. Ma,[9] D. A. Martinez Caicedo,[17] K. T. McDonald,[33] R. D. McKeown,[34,35] Y. Meng,[23] I. Mitchell,[22] J. Monari Kebwaro,[36] Y. Nakajima,[19] J. Napolitano,[37] D. Naumov,[7] E. Naumova,[7] H. Y. Ngai,[29] Z. Ning,[9] J. P. Ochoa-Ricoux,[38] A. Olshevski,[7] H.-R. Pan,[5] J. Park,[23] S. Patton,[19] V. Pec,[30] J. C. Peng,[18] L. E. Piilonen,[23] L. Pinsky,[22] C. S. J. Pun,[29] F. Z. Qi,[9] M. Qi,[8] X. Qian,[4] N. Raper,[39] B. Ren,[27] J. Ren,[24] R. Rosero,[4] B. Roskovec,[30] X. C. Ruan,[24] B. B. Shao,[13] H. Steiner,[28,19] G. X. Sun,[9] J. L. Sun,[40] W. Tang,[4] D. Taychenachev,[7] K. V. Tsang,[19] C. E. Tull,[19] Y. C. Tung,[5] N. Viaux,[38] B. Viren,[4] V. Vorobel,[30] C. H. Wang,[6] M. Wang,[12] N. Y. Wang,[21] R. G. Wang,[9] W. Wang,[32,35] W. W. Wang,[8] X. Wang,[41] Y. F. Wang,[9] Z. Wang,[13] Z. Wang,[9] Z. M. Wang,[9] H. Y. Wei,[13] L. J. Wen,[9] K. Whisnant,[42] C. G. White,[17] L. Whitehead,[22] T. Wise,[2] H. L. H. Wong,[28,19] S. C. F. Wong,[10,32] E. Worcester,[4] Q. Wu,[12] D. M. Xia,[9,43] J. K. Xia,[9] X. Xia,[12] Z. Z. Xing,[9] J. Y. Xu,[10] J. L. Xu,[9] J. Xu,[21] Y. Xu,[25] T. Xue,[13] J. Yan,[36] C. G. Yang,[9] L. Yang,[27] M. S. Yang,[9] M. T. Yang,[12] M. Ye,[9] M. Yeh,[4] B. L. Young,[42] G. Y. Yu,[8] Z. Y. Yu,[9] S. L. Zang,[8] L. Zhan,[9] C. Zhang,[4] H. H. Zhang,[32] J. W. Zhang,[9] Q. M. Zhang,[36] Y. M. Zhang,[13] Y. X. Zhang,[40] Y. M. Zhang,[32] Z. J. Zhang,[27] Z. Y. Zhang,[9] Z. P. Zhang,[31] J. Zhao,[9] Q. W. Zhao,[9] Y. F. Zhao,[14] Y. B. Zhao,[9] L. Zheng,[31] W. L. Zhong,[9] L. Zhou,[9] N. Zhou,[31] H. L. Zhuang,[9] and J. H. Zou[9]

(Daya Bay Collaboration)

[1]*Institute of Modern Physics, East China University of Science and Technology, Shanghai, China*
[2]*University of Wisconsin, Madison, Wisconsin, USA*
[3]*Department of Physics, Yale University, New Haven, Connecticut, USA*
[4]*Brookhaven National Laboratory, Upton, New York, USA*
[5]*Department of Physics, National Taiwan University, Taipei, Taiwan*
[6]*National United University, Miao-Li, Taiwan*
[7]*Joint Institute for Nuclear Research, Dubna, Moscow Region, Russia*
[8]*Nanjing University, Nanjing, China*
[9]*Institute of High Energy Physics, Beijing, China*
[10]*Chinese University of Hong Kong, Hong Kong, China*
[11]*Institute of Physics, National Chiao-Tung University, Hsinchu, Taiwan*
[12]*Shandong University, Jinan, China*
[13]*Department of Engineering Physics, Tsinghua University, Beijing, China*
[14]*North China Electric Power University, Beijing, China*
[15]*Shenzhen University, Shenzhen, China*
[16]*Siena College, Loudonville, New York, USA*
[17]*Department of Physics, Illinois Institute of Technology, Chicago, Illinois, USA*
[18]*Department of Physics, University of Illinois at Urbana-Champaign, Urbana, Illinois, USA*
[19]*Lawrence Berkeley National Laboratory, Berkeley, California, USA*
[20]*Shanghai Jiao Tong University, Shanghai, China*
[21]*Beijing Normal University, Beijing, China*
[22]*Department of Physics, University of Houston, Houston, Texas, USA*
[23]*Center for Neutrino Physics, Virginia Tech, Blacksburg, Virginia, USA*
[24]*China Institute of Atomic Energy, Beijing, China*

[25]School of Physics, Nankai University, Tianjin, China
[26]Department of Physics, University of Cincinnati, Cincinnati, Ohio, USA
[27]Dongguan University of Technology, Dongguan, China
[28]Department of Physics, University of California, Berkeley, California, USA
[29]Department of Physics, The University of Hong Kong, Pokfulam, Hong Kong, China
[30]Charles University, Faculty of Mathematics and Physics, Prague, Czech Republic
[31]University of Science and Technology of China, Hefei, China
[32]Sun Yat-Sen (Zhongshan) University, Guangzhou, China
[33]Joseph Henry Laboratories, Princeton University, Princeton, New Jersey, USA
[34]California Institute of Technology, Pasadena, California, USA
[35]College of William and Mary, Williamsburg, Virginia, USA
[36]Xi'an Jiaotong University, Xi'an, China
[37]Department of Physics, College of Science and Technology, Temple University, Philadelphia, Pennsylvania, USA
[38]Instituto de Física, Pontificia Universidad Católica de Chile, Santiago, Chile
[39]Department of Physics, Applied Physics, and Astronomy, Rensselaer Polytechnic Institute, Troy, New York, USA
[40]China General Nuclear Power Group, China
[41]College of Electronic Science and Engineering, National University of Defense Technology, Changsha, China
[42]Iowa State University, Ames, Iowa, USA
[43]Chongqing University, Chongqing, China

This Letter reports a measurement of the flux and energy spectrum of electron antineutrinos from six 2.9 GW_{th} nuclear reactors with six detectors deployed in two near (effective baselines 512 and 561 m) and one far (1579 m) underground experimental halls in the Daya Bay experiment. Using 217 days of data, 296 721 and 41 589 inverse β decay (IBD) candidates were detected in the near and far halls, respectively. The measured IBD yield is $(1.55 \pm 0.04) \times 10^{-18}$ cm^2 GW^{-1} day^{-1} or $(5.92 \pm 0.14) \times 10^{-43}$ cm^2 fission^{-1}. This flux measurement is consistent with previous short-baseline reactor antineutrino experiments and is 0.946 ± 0.022 (0.991 ± 0.023) relative to the flux predicted with the Huber-Mueller (ILL-Vogel) fissile antineutrino model. The measured IBD positron energy spectrum deviates from both spectral predictions by more than 2σ over the full energy range with a local significance of up to $\sim 4\sigma$ between 4–6 MeV. A reactor antineutrino spectrum of IBD reactions is extracted from the measured positron energy spectrum for model-independent predictions.

Reactor antineutrino experiments have played a key role in developing the picture of neutrinos in the Standard Model of particle physics. They provided the first experimental observation of (anti)neutrinos [1], confirmed neutrino oscillation as the solution to the solar neutrino problem [2], provided the first detection of geoneutrinos [3], and discovered the nonzero neutrino mixing angle θ_{13} [4,5]. Forthcoming reactor antineutrino experiments are aiming to further explore the nature of neutrinos by determining the neutrino mass hierarchy, precisely measuring neutrino mixing parameters, and searching for short-baseline neutrino oscillation [6]. Over the last five decades, reactor antineutrino experiments have measured the flux and spectrum of antineutrinos at various distances from nuclear reactors ranging from ~ 10 m to several hundred kilometers. These measurements were found to be in good agreement [7] with predictions derived from the measurements of the β spectra at ILL [8–10] and Vogel's theoretical calculation [11] when considering the effect of three-neutrino oscillation. In 2011, reevaluations of the reactor antineutrino flux and spectrum with improved theoretical treatments were carried out [12,13], and determined the

flux to be higher than the experimental data. This discrepancy is commonly referred to as the "reactor antineutrino anomaly" [14] and may be a sign of new physics or insufficient fissile antineutrino modeling. Precision measurements by modern reactor antineutrino experiments can shed light on this issue and probe the physics underlying current reactor antineutrino predictions. An accurate determination of the reactor antineutrino spectrum can also provide valuable input to next-generation single-detector reactor antineutrino experiments [15].

This Letter reports measurements of the reactor antineutrino flux and spectrum based on 217 days of data from the Daya Bay experiment. The Daya Bay reactor complex consists of three nuclear power plants (NPPs), each hosting two pressurized-water reactors, which are a common type of commercial thermal reactor. The maximum thermal power of each reactor is 2.9 GW_{th}. The data used for this analysis comprises 338 310 antineutrino candidate events collected in six antineutrino detectors (ADs) in the two near experimental halls (effective baselines 512 m and 561 m) and the one far hall (effective baseline 1579 m). This is the largest sample of reactor antineutrinos, comparable to that

from the BUGEY-4 experiment [16]. A more detailed description of the experimental setup and the data set is given in Ref. [17].

In reactor cores, electron antineutrinos ($\bar{\nu}_e$) are emitted isotropically from fission products of four primary isotopes: ^{235}U, ^{238}U, ^{239}Pu, and ^{241}Pu. The number of $\bar{\nu}_e$ with energy E emitted from a reactor at a time t can be predicted using

$$\frac{d^2\phi(E,t)}{dEdt} = \frac{W_{\text{th}}(t)}{\sum_i f_i(t)e_i} \sum_i f_i(t)S_i(E)c_i^{\text{ne}}(E,t) + S_{\text{SNF}}(E,t),$$

(1)

where the sums are over the four primary isotopes, $W_{\text{th}}(t)$ is the reactor thermal power, $f_i(t)$ is the fraction of fissions due to isotope i, e_i is the average thermal energy released per fission, $S_i(E)$ is the $\bar{\nu}_e$ energy spectrum per fission, $c_i^{\text{ne}}(E,t)$ is the correction to the energy spectrum due to reactor nonequilibrium effects of long-lived fission fragments, and $S_{\text{SNF}}(E,t)$ is the contribution from spent nuclear fuel (SNF). At Daya Bay, the NPPs monitor the reactor power in real time and simulate the evolution of the fuel composition using the SCIENCE software package [18,19]. The measured power (0.5% uncertainty [20–22]) and simulated fission fractions (~5% relative uncertainty [23]) of each core are provided to the Daya Bay Collaboration. The power and fission fractions contributed 0.5% and 0.6% uncertainties to the predicted antineutrino rate, respectively. Simulation of reactor cores based on DRAGON [24] was constructed to study the correlations among the fission fractions of the four isotopes [25]. The energies released per fission (0.2%–0.5% uncertainty) were from Ref. [26]. Nonequilibrium (30% uncertainty) and SNF (100% uncertainty) corrections were applied following Refs. [12] and [27,28], with ~0.5% and ~0.3% contributions to the total antineutrino rate, respectively. The 0.9% total uncertainty in antineutrino flux due to reactor power, fission fractions, and nonequilibrium and SNF corrections was treated to be uncorrelated among reactors in the corresponding oscillation analysis [17]. It is conservatively treated as fully correlated between reactors in this analysis.

Two fissile antineutrino spectrum models were used for $S_i(E)$ in Eq. (1) to predict the reactor antineutrino flux and spectrum. The ILL-Vogel model refers to the conventional ILL model [8–10] of ^{235}U, ^{239}Pu, and ^{241}Pu, and the theoretical model of ^{238}U from Vogel [11]. The Huber-Mueller model refers to the recent reevaluation of ^{235}U, ^{239}Pu, and ^{241}Pu from Huber [13], and that of ^{238}U from Mueller et al. [12]. Both sets of isotope spectra and their uncertainties were taken from the original publications. The Huber-Mueller model was chosen as a reference because of its improved theoretical treatments in β-to-antineutrino

conversions, and the information it provides about uncertainties and their correlations.

Reactor antineutrinos were detected via inverse β decay (IBD) reactions in the gadolinium-doped liquid scintillator (GdLS) of the Daya Bay ADs. The total number of detected IBD events T in a given AD was estimated as

$$T = \sum_{i=1}^{6} \frac{N_P \varepsilon_{\text{IBD}}}{4\pi L_i^2} \iint P_{\text{sur}}(E,L_i)\sigma_{\text{IBD}}(E) \frac{d^2\phi_i(E,t)}{dEdt} dEdt,$$

(2)

where $d^2\phi_i(E,t)/dEdt$ is the differential antineutrino rate from the ith reactor core given in Eq. (1), $\sigma_{\text{IBD}}(E)$ is the cross section of the IBD reaction, L_i is the distance between the center of the detector and the ith core [29], $P_{\text{sur}}(E,L_i)$ is the survival probability due to neutrino oscillation, N_P is the number of target protons [30], and ε_{IBD} is the efficiency of detecting IBD reactions. The cross section $\sigma_{\text{IBD}}(E)$ was evaluated based on the formalism in Ref. [31]. Physical constants including the neutron lifetime (880.3 ± 1.1 s) were taken from the Particle Data Group [32].

IBD candidates were selected by requiring a time coincidence between a prompt signal from an IBD positron including its annihilation energy, and a delayed signal from an IBD neutron after capturing on Gd, as described in Refs. [4,17]. The energy of interacting antineutrinos, E, is closely related to the prompt energy of the IBD positrons, E_{prompt}: without detector effects, $E_{\text{prompt}} \simeq E + (M_p - M_n - M_e) + 2M_e = E - 0.78$ MeV, where M_p, M_n, and M_e are the proton, neutron, and electron masses. The reported data set includes 296 721 and 41 589 IBD candidates at the near and far halls, respectively. Corresponding background rates and spectra were estimated in Ref. [17], with about 5470 ± 240 and 1894 ± 43 background events at the near and far halls, respectively.

The relative analysis of IBD rates for $\sin^2 2\theta_{13}$ requires estimates of uncertainties that are uncorrelated among ADs while the measurement of flux is dominated by uncertainties that are correlated among ADs. A detailed study of the event selection efficiencies was carried out using Monte Carlo (MC) simulation-data comparisons with the Daya Bay simulation framework based on Geant4 [33]. The previous study of efficiencies is described in detail in Ref. [29]. Estimates of each selection efficiency and detector characteristic are summarized in Table I and are briefly described in order below.

Efficiencies of flashing-photomultiplier tube (flasher), capture-time, and prompt-energy selections were determined as described in Ref. [29] utilizing an updated Daya Bay IBD MC simulator. The IBD neutron-Gd capture fraction is dependent on the target's Gd concentration and on the escape, or "spill-out", of IBD neutrons from the target. The former has been measured using neutron calibration sources deployed at the detector center, while the latter was estimated with simulation-data comparisons

TABLE I. Summary of IBD selection efficiencies and their AD-correlated uncertainties. The uncertainties are given in relative units.

	Efficiency (ε)	Uncertainty ($\delta_\varepsilon/\varepsilon$)
Target protons		0.47%
Flasher cut	99.98%	0.01%
Capture-time cut	98.70%	0.12%
Prompt-energy cut	99.81%	0.10%
Gd-capture fraction	84.17%	0.95%
Delayed-energy cut	92.71%	0.97%
Spill-in correction	104.86%	1.50%
Combined	80.6%	2.1%

of source deployments throughout the GdLS volume with a manual calibration system [34]. The efficiency for detecting Gd-capture IBD neutrons, also called the delayed energy cut efficiency, is dependent on the amount of Gd-capture γ energy deposited outside the scintillator and was determined using MC benchmarked to the IBD Gd-capture spectrum from data. Finally, in order to account for contributions from IBD interactions outside the GdLS target, we have applied a spill-in correction determined using simulation-data comparisons of IBD coincidence time and reconstructed position distributions. The updated detector efficiency ε was estimated to be 80.6% with an AD-correlated fractional uncertainty $\delta_\varepsilon/\varepsilon$ of 2.1%. Application of additional AD-dependent muon veto and multiplicity cut efficiencies, described in detail in Refs. [17,29], produced total detection efficiencies ε_{IBD} ranging from 64.6% to 77.2% among ADs. The total correlated uncertainty was dominated by the spill-in correction, whose uncertainty enveloped the individual uncertainties provided by three independent methods and was limited by small biases in position reconstruction. A cross-check of the spill-in effect provided by data-simulation comparisons of neutron sources deployed outside the target volume showed agreement well within this uncertainty.

To extract the rate of IBD interactions at Daya Bay, the θ_{13}-driven oscillation effect must be corrected for in each detector. A normalization factor R was defined to scale the measured rate to that predicted with a fissile antineutrino spectrum model. The value of R, together with the value of $\sin^2 2\theta_{13}$, were simultaneously determined with a χ^2 similar to the one used in Ref. [4]:

$$\chi^2 = \sum_{d=1}^{6} \frac{[M_d - RT_d(1 + \epsilon_D + \sum_r \omega_r^d \alpha_r + \epsilon_d) + \eta_d]^2}{M_d + B_d}$$

$$+ \sum_r \frac{\alpha_r^2}{\sigma_r^2} + \sum_{d=1}^{6} \left(\frac{\epsilon_d^2}{\sigma_d^2} + \frac{\eta_d^2}{\sigma_{B_d}^2} \right) + \frac{\epsilon_D^2}{\sigma_D^2}, \qquad (3)$$

where M_d is the number of measured IBD events in the dth detector with backgrounds subtracted, B_d is the

corresponding number of background events, T_d is the number of IBD events predicted with a fissile antineutrino spectrum model via Eq. (2), and ω_r^d is the fractional IBD contribution from the rth reactor to the dth detector determined with baselines and reactor antineutrino rates, σ_r (0.9%) is the uncorrelated reactor uncertainty, σ_d (0.2% [17]) is the uncorrelated detection uncertainty, σ_{B_d} is the background uncertainty listed in Ref. [17], and σ_D (2.1%) is the correlated detection uncertainty, i.e., the uncertainty of detection efficiency in Table I. Their corresponding nuisance parameters are α_r, ϵ_d, η_d, and ϵ_D, respectively. The best-fit value of $\sin^2 2\theta_{13} = 0.090 \pm 0.009$ is insensitive to the choice of model. The best-fit value of R is 0.946 ± 0.022 (0.991 ± 0.023) when predicting with the Huber-Mueller (ILL-Vogel) model. Replacing the Mueller ^{238}U spectrum with the recently measured spectrum in Ref. [35] yields negligible change in R. The uncertainty in R is dominated by the correlated detection uncertainty σ_D.

With the oscillation effect for each AD corrected using the best-fit value of $\sin^2 2\theta_{13}$ in Eq. (3), the measured IBD yield for each AD is expressed in two ways: the yield per GW$_{\text{th}}$ per day, Y, and equivalently, the yield per nuclear fission, σ_f. These results are shown in the top panel of Fig. 1. The measured IBD yields are consistent among all ADs after further correcting for the small variations of fission fractions among the different sites. The average IBD yield in the three near ADs is $Y = (1.55 \pm 0.04) \times 10^{-18}$ cm^2 GW^{-1} day^{-1}, or $\sigma_f = (5.92 \pm 0.14) \times 10^{-43}$ cm^2 fission^{-1}. These results are summarized in Table II along with the flux-weighted average fission fractions in the three near ADs.

A global fit for R was performed to compare with previous reactor antineutrino flux measurements following the method described in Ref. [36]. Nineteen past short-baseline (<100 m) measurements were included using the data from Ref. [14]. The measurements from Chooz [37] and Palo Verde [38] were also included after correcting for the effect of standard three-neutrino oscillations. All measurements were compared to the Huber-Mueller model. All predictions were fixed at their nominal value in the fit. The resulting past global average is $R_g^{\text{past}} = 0.942 \pm 0.009(\text{expt}) \pm 0.025(\text{model})$. Daya Bay's measurement of the reactor antineutrino flux is consistent with the past experiments. Including Daya Bay in the global fit, the new average is $R_g = 0.943 \pm 0.008(\text{expt}) \pm 0.025(\text{model})$. The results of the global fit are shown in the bottom panel of Fig. 1.

Extending the study from the integrated flux to the energy spectrum, the measured prompt-energy spectra of the three near-site ADs were combined after background subtraction and compared with predictions. The antineutrino spectrum at each detector was predicted by the procedure described above, taking into account neutrino oscillation with $\sin^2 2\theta_{13} = 0.090$ and $\Delta m_{ee}^2 = 2.59 \times 10^{-3}$ eV^2 based on the oscillation analysis of the same
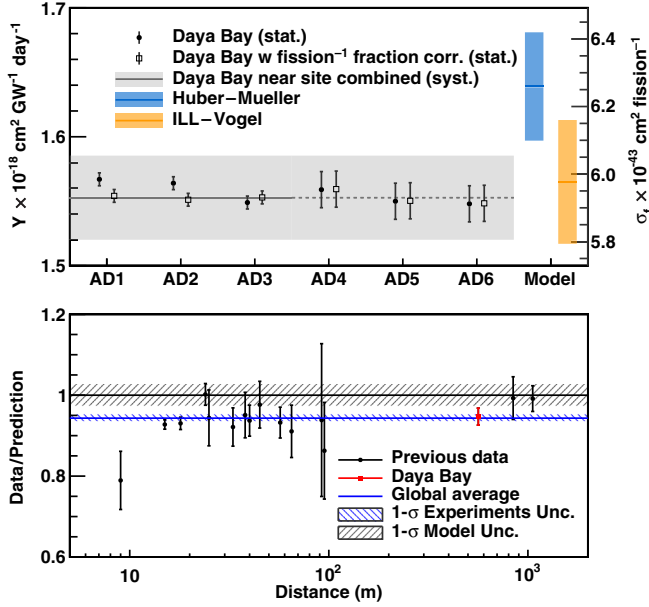
FIG. 1.   Top: Rate of reactor antineutrino candidate events in the six ADs with corrections for three-flavor oscillations (closed circles), and additionally for the variation of flux-weighted fission fractions at the different sites (open squares). The average of the three near detectors is shown as a gray line (and extended through the three far detectors as a dotted gray line) with its 1σ systematic uncertainty (gray band). The rate predicted with the Huber-Mueller (ILL-Vogel) model and its uncertainty are shown in blue (orange). Bottom: The measured reactor $\bar{\nu}_e$ rate as a function of the distance from the reactor, normalized to the theoretical prediction with the Huber-Mueller model. The rate is corrected for three-flavor neutrino oscillations at each baseline. The blue shaded region represents the global average and its 1σ uncertainty. The 2.7% model uncertainty is shown as a band around unity. Measurements at the same baseline are combined for clarity. The Daya Bay measurement is shown at the flux-weighted baseline (573 m) of the two near halls.

data [17]. The detector response was determined in two ways. The first method sequentially applied a simulation of energy loss in the inactive acrylic vessels, and analytical models of energy scale and energy resolution. The energy scale model was based on empirical characterization of the

TABLE II.   Average IBD yields (Y and σ_f) of the near halls, flux normalization with respect to different fissile antineutrino model predictions, and flux-weighted average fission fractions of the near halls.

IBD Yield	
Y (cm^2 GW^{-1} day^{-1})	$(1.55 \pm 0.04) \times 10^{-18}$
σ_f (cm^2 fission^{-1})	$(5.92 \pm 0.14) \times 10^{-43}$
Data/Prediction	
R (Huber-Mueller)	0.946 ± 0.022
R (ILL-Vogel)	0.991 ± 0.023
Average Fission Fractions	
^{235}U: ^{238}U: ^{239}Pu: ^{241}Pu	0.586: 0.076: 0.288: 0.050

spatial nonuniformity and the energy nonlinearity with improved calibration of the scintillator light yield and the electronics response [39]. The uncertainty of the energy scale was about 1% in the energy range of reactor antineutrinos [39]. The second method used full-detector simulation in which the detector response was tuned with the calibration data. Both methods produced consistent predictions for prompt energies above 1.25 MeV. Around 1 MeV, there was a slight discrepancy due to different treatments of IBD positrons that interact with the inner acrylic vessels. Additional uncertainty below 1.25 MeV was included to cover this discrepancy.

Figure 2 shows the observed prompt-energy spectrum and its comparison with the predictions. The predicted spectra were normalized to the measurement in order to test the agreement between spectral shapes. The spectral uncertainty of the measurement is composed of the statistical, detector response and background uncertainties. Between 1.5 and 7 MeV, it ranges from 1.0% at 3.5 MeV to
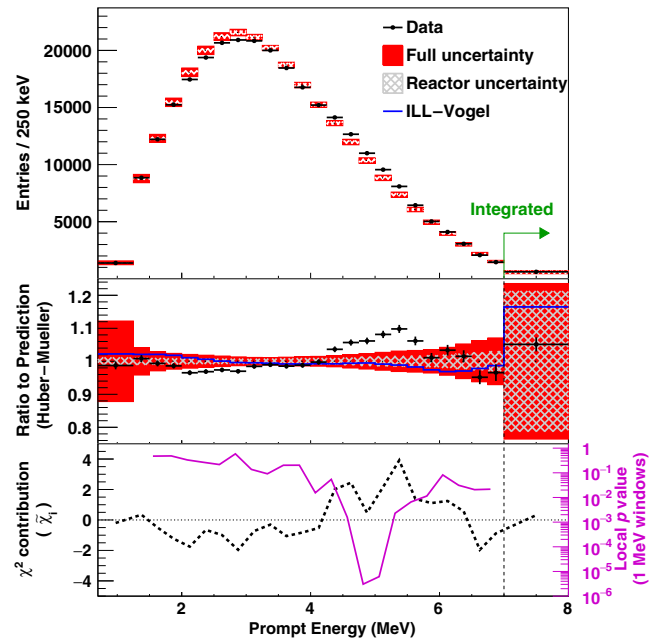

FIG. 2.   Top panel: Predicted and measured prompt-energy spectra. The prediction is based on the Huber-Mueller model and normalized to the number of measured events. The highest energy bin contains all events above 7 MeV. The gray hatched and red filled bands represent the square root of diagonal elements of the shape-only covariance matrix ($\sqrt{V_{ii}}$) for the reactor related and the full (reactor, detector, and background) systematic uncertainties, respectively. The error bars on the data represent the statistical uncertainty. Middle panel: Ratio of the measured prompt-energy spectrum to the predicted spectrum (Huber-Mueller model). The blue curve shows the ratio of the prediction based on the ILL-Vogel model to that based on the Huber-Mueller model. Bottom panel: The defined χ^2 distribution ($\tilde{\chi}_i$) of each bin (black dashed curve) and local p values for 1-MeV energy windows (magenta solid curve). See the text for the definitions of these quantities.

6.7% at 7 MeV, and above 7 MeV, it is larger than 10%. Agreement between a prediction and the data was quantified with the χ^2 defined as

$$\chi^2 = \sum_{i,j}(N_i^{\mathrm{obs}} - N_i^{\mathrm{pred}})V_{ij}^{-1}(N_j^{\mathrm{obs}} - N_j^{\mathrm{pred}}), \qquad (4)$$

where $N_i^{\mathrm{obs(pred)}}$ is the observed (predicted) number of events at the ith prompt-energy bin and V is the covariance matrix that includes all statistical and shape-only systematic uncertainties. The systematic uncertainty portion of the covariance matrix V was estimated using simulated data sets with randomly fluctuated detector response, background contributions, and reactor-related uncertainties, while the statistical uncertainty portion was calculated analytically. A comparison to the Huber-Mueller model yielded a χ^2/NDF, where NDF is the number of degrees of freedom, of 43.0/24 in the full energy range from 0.7 to 12 MeV, corresponding to a 2.6σ discrepancy. The ILL-Vogel model showed a similar level of discrepancy from the data at 2.4σ.

The ratio of the measured to predicted prompt-energy spectra is shown in the middle panel of Fig. 2. A discrepancy is apparent around 5 MeV. Two approaches were adopted to evaluate the significance of local discrepancies. The first was based on the χ^2 contribution of each energy bin, which is evaluated by

$$\tilde{\chi}_i = \frac{N_i^{\mathrm{obs}} - N_i^{\mathrm{pred}}}{|N_i^{\mathrm{obs}} - N_i^{\mathrm{pred}}|}\sqrt{\sum_j \chi_{ij}^2},$$

where $\chi_{ij}^2 \equiv (N_i^{\mathrm{obs}} - N_i^{\mathrm{pred}})V_{ij}^{-1}(N_j^{\mathrm{obs}} - N_j^{\mathrm{pred}})$. (5)

As shown in the bottom panel of Fig. 2, there is a larger contribution around 5 MeV. In the second approach, the significance of deviations are conveyed with p values calculated within local energy windows. A free-floating nuisance parameter for the normalization of each bin within a chosen energy window was introduced to the fitter that was used in the neutrino oscillation analysis [17]. The overall normalization was unconstrained in the fit. The difference in the minimum χ^2 before and after introducing these nuisance parameters was used to evaluate the p value of the deviation from the theoretical prediction within each window. The p values within 1-MeV energy windows are shown in the bottom panel of Fig. 2. The p value for a 2-MeV window between 4 and 6 MeV reached a similar minimum of 5.4×10^{-5}, which corresponds to a 4.0σ deviation. The ILL-Vogel model showed a similar level of discrepancy between 4 and 6 MeV.

The number of events in excess of the predictions in the 4–6 MeV region was estimated to comprise approximately 1%–2% of all events in both the near and far detectors. This excess is approximately 10% of events within the 4–6 MeV region. This discrepancy was found to be time independent and correlated with reactor power, therefore disfavoring

hypotheses involving unknown backgrounds. The hypothesis that the excess was due to detector response was disfavored given that no discrepancy was observed in the ^{12}B spectrum [17]. A similar excess was observed in other reactor antineutrino experiments [40,41]. A recent *ab initio* calculation of the antineutrino spectrum showed a similar deviation from previous predictions in the 4–6 MeV region and identified prominent fission daughter isotopes as a potential explanation [42]. A number of tentative explanations based on the nuclear physics of β decays and fission yields have been put forward and are under active investigation; for examples, see Refs. [42–46]. These studies suggest an increased uncertainty in both the yields and spectra of the fissile antineutrino models, which may also account for the discrepancy.

From the measured IBD prompt spectrum at Daya Bay, we have obtained a reactor antineutrino spectrum of IBD reactions that can be used to make model-independent predictions of reactor antineutrino flux and spectra [47]. The spectrum was obtained by first summing the prompt-energy spectra of the three near site ADs weighted with their target mass relative to the average target mass of all near-site ADs, $\bar{M}$: $S_{\mathrm{combined}}(E_{\mathrm{prompt}}) = \sum_{i=1}^{3}S_i(E_{\mathrm{prompt}})\bar{M}/M_i$. Detector response effects were then removed by unfolding the combined prompt spectrum $S_{\mathrm{combined}}(E_{\mathrm{prompt}})$ to an antineutrino spectrum of IBD reactions, $S_{\mathrm{combined}}(E)$. Finally, oscillation effects were removed and each bin of the antineutrino spectrum was normalized to $\mathrm{cm}^2\,\mathrm{fission}^{-1}\,\mathrm{MeV}^{-1}$ using the thermal power $W_{\mathrm{th}}(t)$ and fission fraction $f_i(t)$ information of each core. The reactor antineutrino spectrum is expressed as

$$S_{\mathrm{reactor}}(E) = \frac{S_{\mathrm{combined}}(E)}{\bar{P}_{\mathrm{sur}}(E)\bar{N}_P \cdot F_{\mathrm{total}}}, \qquad (6)$$

where $\bar{P}_{\mathrm{sur}}(E)$ is the flux-weighted average of the survival probabilities $P_{\mathrm{sur}}(E, L_{i,d})$ from the six reactors (i) to the three detectors (d), $\bar{N}_P$ is the number of target protons in $\bar{M}$, and F_{total} is the total number of fissions from the sum of the fissions of the six reactors to the three detectors weighted with $\varepsilon_{\mathrm{IBD},d}/4\pi L_{i,d}^2$. Correcting the unfolded spectrum with an average survival probability resulted in a negligible bias ($< 0.01\%$).

Detector response effects were removed with the singular value decomposition (SVD) unfolding method [48]. Statistical and systematical uncertainties are naturally propagated in the SVD method. The bias of unfolding was estimated by using detector response matrices constructed from the two different detector response models and by using a variety of input antineutrino spectra which covered the uncertainties of the two models and those estimated in Ref. [42]. The bin-to-bin bias between 2.2 and 6.5 MeV was about 0.5%, which was a few times smaller than the statistical uncertainty. The bias outside this region was about 4% and increased with energy due to the
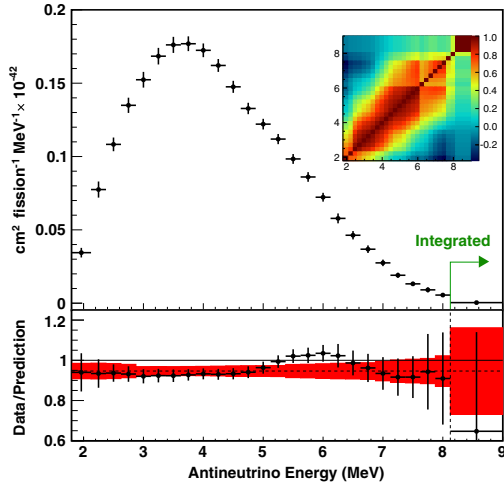
FIG. 3.   Top panel: The extracted reactor antineutrino spectrum
and its correlation matrix. Bottom panel: Ratio of the extracted
reactor antineutrino spectrum to the Huber-Mueller prediction.
The error bars of the data points are the square roots of the
diagonal elements of the data covariance matrix, which included
statistical and systematic uncertainties, as well as bias and the
AD-correlated uncertainty from Table I. The solid red band
represents the square roots of the diagonal elements of the
prediction covariance matrix, which included reactor and
Huber-Mueller model uncertainties. The horizontal dashed line
represents the normalization factor $R = 0.946$. The vertical
dashed line denotes that above 8 MeV, the Huber-Mueller model
was extrapolated.

decrease of events. The bias values were assigned as addi-
tional uncertainties to the unfolded spectrum. Unfolding
performed with the Bayesian iteration method [49,50]
produced consistent results. Between 2 and 7.5 MeV, the
spectral uncertainty of the unfolded spectrum $S_{\text{combined}}(E)$
ranges from 1.1% at 4.25 MeV to 9.3% at 7.5 MeV, and
around 10 MeV is more than 20% due to low statistics. The
obtained reactor antineutrino spectrum and its correlation
matrix are shown in the top panel of Fig. 3. Between 2
and 7.5 MeV, the uncertainty of the diagonal elements
ranges from 2.7% at 4.25 MeV to 10.4% at 7.5 MeV. The
bottom panel of Fig. 3 is the ratio of the extracted reactor
antineutrino spectrum to the prediction using the fissile
antineutrino spectra of the Huber-Mueller model and the
average fission fractions listed in Table II. The integral of
the ratio is equal to the flux normalization factor R given in
Table II. The integral of the spectrum is equal to the yield
σ_f given in Table II. The discrepancy between 5 and 7 MeV
corresponds to the discrepancy between 4 and 6 MeV in the
IBD prompt-energy distribution in Fig. 2.

In summary, the Daya Bay experiment collected
more than 330 000 antineutrino events in the data-taking
period with six antineutrino detectors. The measured
IBD yield is $(1.55 \pm 0.04) \times 10^{-18}$ cm^2 GW^{-1} day^{-1} or
$(5.92 \pm 0.14) \times 10^{-43}$ cm^2 fission^{-1}. This flux measure-
ment is consistent with the global average of previous

short baseline experiments and is 0.946 ± 0.022 (0.991 ± 0.023) times the prediction using the Huber-Mueller
(ILL-Vogel) fissile antineutrino model. In addition, the
measured and predicted spectra are discrepant with a
significance of $\sim 4\sigma$ in the 4–6 (5–7) MeV region of the
IBD prompt (antineutrino) energy spectrum. Investigation
of the discrepancy strongly disfavors explanations involv-
ing detector response or an unknown background. A reactor
antineutrino spectrum was extracted from the measurement
at Daya Bay, enabling model-independent predictions of
reactor antineutrino spectra.

[1] C. L. Cowan, F. Reines, F. B. Harrison, H. W. Kruse, and
    A. D. McGuire, Science **124**, 103 (1956).
[2] K. Eguchi *et al.*, Phys. Rev. Lett. **90**, 021802 (2003).
[3] T. Araki *et al.*, Nature (London) **436**, 499 (2005).
[4] F. P. An *et al.* (Daya Bay Collaboration), Phys. Rev. Lett.
    108, 171803 (2012).
[5] J. K. Ahn *et al.* (RENO Collaboration), Phys. Rev. Lett. **108**,
    191802 (2012).
[6] P. Vogel, L. Wen, and C. Zhang, Nat. Commun. **6**, 6935
    (2015).
[7] C. Bemporad, G. Gratta, and P. Vogel, Rev. Mod. Phys. **74**,
    297 (2002).
[8] K. Schreckenbach, G. Colvin, W. Gelletly, and F. Von
    Feilitzsch, Phys. Lett. **160B**, 325 (1985).

[9] F. Von Feilitzsch, A. A. Hahn, and K. Schreckenbach, Phys. Lett. **118B**, 162 (1982).

[10] A. A. Hahn, K. Schreckenbach, W. Gelletly, F. von Feilitzsch, G. Colvin, and B. Krusche, Phys. Lett. B **218**, 365 (1989).

[11] P. Vogel, G. K. Schenter, F. M. Mann, and R. E. Schenter, Phys. Rev. C **24**, 1543 (1981).

[12] T. A. Mueller et al., Phys. Rev. C **83**, 054615 (2011).

[13] P. Huber, Phys. Rev. C **84**, 024617 (2011).

[14] G. Mention, M. Fechner, Th. Lasserre, Th. A. Mueller, D. Lhuillier, M. Cribier, and A. Letourneau, Phys. Rev. D **83**, 073006 (2011).

[15] F. P. An et al. (JUNO collaboration), arXiv:1507.05613.

[16] Y. Declais et al., Phys. Lett. B **338**, 383 (1994).

[17] F. P. An et al. (Daya Bay Collaboration), Phys. Rev. Lett. **112**, 061801 (2014).

[18] S. Rauck, Framatome ANP Document No. NFPSD/DC/89 **14** (2004).

[19] R. Sanchez et al., Nucl. Eng. Tech. **42**, 474 (2010).

[20] J. Cao, Nucl. Phys. B, Proc. Suppl. **229**–**232**, 205 (2012).

[21] S. F. E. Tournu et al., EPRI Report No. EPRI 2001.1001470, 2001.

[22] C. R. Xu et al., Chin. J. Nucl. Sci. Eng. **23**, 26 (2003).

[23] APOLLO2: Vailidation/Qualification, http://nucleaire-saclay.cea.fr/Phocea/Vie_des_labos/Ast/ast_technique.php?id_ast=351.

[24] R. R. G. Marleau, A. Hebert, and R. Roy, Report No. **IGE-236**, 2001.

[25] X. B. Ma, L. Z. Wang, Y. X. Chen, W. L. Zhong, and F. P. An, arXiv:1405.6807.

[26] V. Kopeikin, L. Mikaelyan, and V. Sinev, Phys. At. Nucl. **67**, 1892 (2004).

[27] F. P. An, X. C. Tian, L. Zhan, and J. Cao, Chin. Phys. C **33**, 711 (2009).

[28] B. Zhou, X.-C. Ruan, Y.-B. Nie, Z.-Y. Zhou, F.-P. An, and J. Cao, Chin. Phys. C **36**, 1 (2012).

[29] F. P. An et al. (Daya Bay Collaboration), Chin. Phys. C **37**, 011001 (2013).

[30] See Supplemental Material at http://link.aps.org/supplemental/10.1103/PhysRevLett.116.061801 for supplied values.

[31] P. Vogel and J. F. Beacom, Phys. Rev. D **60**, 053003 (1999).

[32] K. A. Olive et al. (Particle Data Group), Chin. Phys. C **38**, 090001 (2014).

[33] S. Agostinelli et al. (GEANT4 Collaboration), Nucl. Instrum. Methods Phys. Res., Sect. A **506**, 250 (2003).

[34] H. X. Huang et al., J. Instrum. **8**, P09013 (2013).

[35] N. Haag, A. Gütlein, M. Hofmann, L. Oberauer, W. Potzel, K. Schreckenbach, and F. M. Wagner, Phys. Rev. Lett. **112**, 122501 (2014).

[36] C. Zhang, X. Qian, and P. Vogel, Phys. Rev. D **87**, 073018 (2013).

[37] M. Apollonio et al., Phys. Lett. B **466**, 415 (1999).

[38] F. Boehm et al., Phys. Rev. D **64**, 112001 (2001).

[39] F. P. An et al. (Daya Bay Collaboration), Phys. Rev. Lett. **115**, 111802 (2015).

[40] Y. Abe et al. (Double Chooz Collaboration), J. High Energy Phys. 10 (2014) 086; J. High Energy Phys. 02 (2015) 74.

[41] S.-H. Seo (RENO Collaboration), AIP Conf. Proc. **1666**, 080002 (2015).

[42] D. A. Dwyer and T. J. Langford, Phys. Rev. Lett. **114**, 012502 (2015).

[43] A. A. Sonzogni, T. D. Johnson, and E. A. McCutchan, Phys. Rev. C **91**, 011301 (2015).

[44] A. C. Hayes, J. L. Friar, G. T. Garvey, G. Jungman, and G. Jonkmans, Phys. Rev. Lett. **112**, 202501 (2014).

[45] A. A. Zakari-Issoufou et al. (IGISOL collaboration), Phys. Rev. Lett. **115**, 102503 (2015).

[46] A. C. Hayes, J. L. Friar, G. T. Garvey, D. Ibeling, G. Jungman, T. Kawano, and R. W. Mills, Phys. Rev. D **92**, 033015 (2015).

[47] See Supplemental Material at http://link.aps.org/supplemental/10.1103/PhysRevLett.116.061801 for an example.

[48] A. Hocker and V. Kartvelishvili, Nucl. Instrum. Methods Phys. Res., Sect. A **372**, 469 (1996).

[49] G. D'Agostini, Nucl. Instrum. Methods Phys. Res., Sect. A **362**, 487 (1995).

[50] T. Adye, Proceedings of the PHYSTAT 2011 Workshop, CERN, Geneva, Switzerland, 2011 (Report No. CERN-2011-006), p. 313.